

# Optimized synthesis method for K/Co<sub>3</sub>O<sub>4</sub> catalyst towards direct decomposition of N<sub>2</sub>O

Hiroaki Yoshino · Chie H. Ohnishi ·  
Saburo Hosokawa · Kenji Wada · Masashi Inoue

Received: 27 February 2010 / Accepted: 5 August 2010 / Published online: 24 August 2010  
© Springer Science+Business Media, LLC 2010

**Abstract** The potassium-doped Co<sub>3</sub>O<sub>4</sub> catalysts were prepared by impregnation of potassium sources on commercial cobalt carbonate and on the precursors synthesized by homogeneous precipitation, combustion with glycine, gradual oxidation, and hydrothermal methods. The activities of these catalysts for the direct decomposition of nitrous oxide in the presence of oxygen with or without water vapor were examined. The effects of potassium sources on the catalyst activity were also examined by impregnation of various potassium salts on commercial cobalt carbonate. The catalyst prepared by impregnation of an aqueous solution of KOH on commercial cobalt carbonate showed the highest activity. The catalysts prepared by various methods were analyzed by powder X-ray diffraction, N<sub>2</sub> adsorption, scanning electron microscope, temperature-programmed reduction with H<sub>2</sub>, temperature-programmed desorption of O<sub>2</sub>, and X-ray photoelectron spectroscopy. These results suggest that crystallite size and reduction property are key factors for the activity of the catalyst for the direct decomposition of nitrous oxide in the presence of oxygen.

## Introduction

Recently, catalytic removal of nitrous oxide (N<sub>2</sub>O) from industrial exhaust has attracted much attention, because N<sub>2</sub>O has been reported to have a significant global

warming potential 310 times larger than that of CO<sub>2</sub> [1] and to contribute to the destruction of the ozone layer in the stratosphere [2]. So far, noble metals [2–6], metal oxides [7–11], and ion-exchanged zeolites [12–14] have been reported to exhibit catalytic activity towards the direct decomposition of nitrous oxide (Eq. 1). Besides N<sub>2</sub>O abatement from exhaust gases, catalytic decomposition of N<sub>2</sub>O was also proposed as the propulsion system for small spacecrafts [15, 16].



The significant anthropogenic sources of N<sub>2</sub>O are nitric acid plants and adipic acid plants. However, the N<sub>2</sub>O concentration in the tail gases from the adipic acid plants is relatively high (20–60%) [17], and thermal decomposition of N<sub>2</sub>O [17, 18] may be more economical because this method gives NO, besides N<sub>2</sub> and O<sub>2</sub>, from which nitric acid, the oxidizing agent for the formation of adipic acid from the mixture of cyclohexanol and cyclohexanone, can be regenerated. For the tail gases from the nitric acid plants, catalytic decomposition seems to be a suitable solution [13, 19].

Excellent catalytic activities of cobalt oxides for N<sub>2</sub>O abatement have been long recognized. Early works took notice of the activity of CoO [20–22]. However, its activity readily deteriorated because of the oxidation of the catalyst by N<sub>2</sub>O [21].

Then, cobalt-based catalysts derived from hydrotalcites gathered much attention because spinel catalysts having large surface areas and high thermal stabilities can be easily prepared from the hydrotalcites obtained by co-precipitation methods [23–25]. Various catalyst systems prepared by this route have been proposed such as Co–Al [23, 24], Co–Mg [25, 26], Co–Ni [26], Co–Zn [27], and Co–Mn [28].

H. Yoshino · C. H. Ohnishi · S. Hosokawa · K. Wada ·  
M. Inoue (✉)  
Department of Energy and Hydrocarbon Chemistry,  
Graduate School of Engineering, Kyoto University,  
Katsura, Kyoto 615-8510, Japan  
e-mail: inoue@scl.kyoto-u.ac.jp

In patent literature, Armor et al. [29] claimed that the addition of  $\text{Na}^+$  ions to the catalyst derived from a Co–Al hydrotalcite significantly increased the  $\text{N}_2\text{O}$  decomposition activity of the catalyst. Pérez-Ramírez et al. [30] noted that the de $\text{N}_2\text{O}$  activity of a Co–Rh, Al catalyst was considerably affected by  $\text{Na}^+$  ions remaining in the catalyst from the co-precipitation step for the synthesis of the hydrotalcite precursor. Unfortunately, this description has not drawn attention of the de $\text{N}_2\text{O}$  researchers, because main theme of their paper is to propose the dual-bed system for  $\text{NO}_x$  removal from the flue gases from lean-burn engines.

We found that when precursors were prepared by precipitation of  $\text{Co}(\text{NO}_3)_2$  with  $\text{Na}_2\text{CO}_3$  and were thoroughly washed, the alkali content in the  $\text{Co}_3\text{O}_4$  catalyst depended on the crystal structure of the precursor, thus precipitation conditions affecting the catalyst activity [31]. The  $\text{Co}_3\text{O}_4$  catalyst promoted by a proper amount of alkali ions is quite effective for the direct decomposition of  $\text{N}_2\text{O}$  in the presence of oxygen [32], maintaining its activity at least for 12 h in the presence of both oxygen and water. The addition of alkali ions to  $\text{Co}_3\text{O}_4$  was found to promote the regeneration of  $\text{Co}^{2+}$  from  $\text{Co}^{3+}$  formed during  $\text{N}_2\text{O}$  decomposition [33]. Simultaneously, Xue et al. [34] reported the promotion effect of residual  $\text{Na}^+$  ion on the activity of Co–Ce catalyst prepared by co-precipitation using  $\text{K}_2\text{CO}_3$  as a precipitant. Since then, many papers have reported excellent promoting effects of alkali or alkaline earth components on the de $\text{N}_2\text{O}$  activity of cobalt-based catalysts [35–41]. Note that excellent activities of alkali-promoted  $\text{Co}_3\text{O}_4$  catalysts for the direct decomposition of NO were also reported by Park et al. [42] and Haneda et al. [43].

As mentioned above, preparation method for the alkali-promoted  $\text{Co}_3\text{O}_4$  catalyst significantly affects its activity for  $\text{N}_2\text{O}$  decomposition; however, such effects have not been systematically investigated so far. In the present study, therefore, we have optimized the preparation method for the potassium-doped  $\text{Co}_3\text{O}_4$  catalyst by changing the precursors of  $\text{Co}_3\text{O}_4$  and potassium sources to maximize the activity for the direct decomposition of nitrous oxide in the presence of oxygen and/or water vapor. The results presented here clearly suggest that several key factors govern the activity of the catalyst.

## Experimental section

### Preparation of K-doped $\text{Co}_3\text{O}_4$ catalysts

Catalysts were prepared by: (a) impregnation of commercial cobalt(II) carbonate [32, 33], (b) homogeneous precipitation [44], (c) combustion with glycine [45],

(d) gradual oxidation [46], and (e) hydrothermal synthesis [47]. The details are as follows.

#### (a) Impregnation of commercial cobalt(II) carbonate [32, 33]

Commercial cobalt(II) carbonate (Nacalai Tesque, 0.020 mol) was impregnated with an aqueous solution (2  $\text{cm}^3$ ) of  $\text{KNO}_3$  (Wako,  $4.0 \times 10^{-4}$  mol; atomic ratio of K/Co, 0.02) on an 80 °C water bath, and the  $\text{K}/\text{Co}_3\text{O}_4$  catalyst was obtained by the calcination of the dried powder at 400 °C for 4 h in air. The catalyst is designated as catalyst **A**.

For comparison, cobalt oxide, which was prepared by the calcination of commercial cobalt(II) carbonate at 400 °C in air for 4 h, was impregnated with an aqueous solution (2  $\text{cm}^3$ ) of  $\text{KNO}_3$  ( $4.0 \times 10^{-4}$  mol; atomic ratio of K/Co, 0.02) at 80 °C followed by drying and calcination at 400 °C for 1 h in air to give catalyst **A'**.

#### (b) Homogeneous precipitation [44]

Cobalt nitrate hexahydrate ( $\text{Co}(\text{NO}_3)_3 \cdot 6\text{H}_2\text{O}$ ; Wako, 0.050 mol) and urea (Wako, 0.10 mol) were dissolved in deionized water (750  $\text{cm}^3$ ). The mixture was heated in an oil bath. The bath temperature was increased from room temperature to 120 °C and kept at 120 °C for 2 h. After the mixture had been cooled, the resulting powder was washed with deionized water three times and with methanol once by centrifuging and then air-dried. The resulting precursor was impregnated with an aqueous  $\text{KNO}_3$  solution (0.20 M; K/Co = 0.02), dried at 80 °C, and calcined at 400 °C in air for 4 h. This sample is called catalyst **B**.

#### (c) Combustion with glycine [45]

Cobalt nitrate hexahydrate, glycine (Nacalai Tesque) and  $\text{KNO}_3$  were dissolved in a small amount of deionized water. The glycine/Co molar ratio was 1.2, and K/Co molar ratio was 0.02. The mixed solution was heated on an electric hot plate kept at 300 °C. When vigorous reaction started, heating was stopped. The product was calcined at 400 °C for 4 h in air. This sample is designated as catalyst **C**.

#### (d) Gradual oxidation [46]

In a three-necked flask, NaOH (0.030 mol) and  $\text{NaNO}_3$  (1.0 mol) were dissolved in deionized water (100  $\text{cm}^3$ ), and 1.0 M aqueous  $\text{Co}(\text{NO}_3)_2$  solution (20  $\text{cm}^3$ ) was added gradually over a period of 45 s. The mixture was kept in a 95 °C oil bath for 42 h with bubbling of air (70  $\text{cm}^3 \text{min}^{-1}$ ). After the mixture had been cooled, the

resulting powder was washed with deionized water three times and with methanol once by centrifuging and then air-dried. The thus-obtained precursor was impregnated with a  $\text{KNO}_3$  solution ( $\text{K/Co} = 0.02$ ), dried, and calcined at  $400\text{ }^\circ\text{C}$  for 4 h as described above (catalyst **D**).

#### (e) Hydrothermal synthesis [47]

Cobalt chloride hexahydrate ( $\text{CoCl}_2 \cdot 6\text{H}_2\text{O}$ ; Wako, 0.019 mol) and urea (0.019 mol) were dissolved in deionized water ( $190\text{ cm}^3$ ) and the solution was placed in a Teflon autoclave. Then, the autoclave was sealed and kept at  $100\text{ }^\circ\text{C}$  for 12 h. After the mixture had been cooled, the resulting powder was washed three times with deionized water and with methanol once by centrifuging and then air-dried. Following the method for preparation of catalyst **A**, the precursor was impregnated with an aqueous solution of  $\text{KNO}_3$  ( $\text{K/Co} = 0.02$ ) and calcined at  $400\text{ }^\circ\text{C}$  for 4 h (catalyst **E**).

#### Catalyst activity test

Catalyst tests were carried out in a fixed-bed flow reactor. The catalyst was tabletted, pulverized into 10–22 mesh, and set in the reactor. The catalyst bed was heated to  $500\text{ }^\circ\text{C}$  and held at that temperature for 30 min in a helium flow. Then, the reaction gas composed of 5000 ppm  $\text{N}_2\text{O}$ , 2.0%  $\text{O}_2$ , 0 or 2.5%  $\text{H}_2\text{O}$ , and He balance was introduced to the catalyst bed at  $W/F = 0.30\text{ g s cm}^{-3}$ . The effluent gases from the reactor were analyzed every 5 min with an on-line micro gas-chromatograph (CP 2002, Chrompack, Netherlands) (columns: 10 m Molecular Sieve 5A at  $80\text{ }^\circ\text{C}$ ; 10 m Porapack Q at  $40\text{ }^\circ\text{C}$ ). After the steady state was attained, reaction temperature was decreased, and the catalyst performance was measured at every  $50\text{ }^\circ\text{C}$  from  $500\text{ }^\circ\text{C}$  to the temperature where  $\text{N}_2\text{O}$  conversion was negligible.

#### Characterization of the catalysts

Powder X-ray diffraction (XRD) pattern was recorded on a Shimadzu XD-D1 diffractometer using  $\text{Cu K}\alpha$  radiation through a carbon monochromator. The crystallite size of  $\text{Co}_3\text{O}_4$  was calculated from the full width at half maximum (FWHM) of the diffraction peak at around  $65^\circ$  ( $2\theta$ ) using Scherrer equation:

$$D\text{ (nm)} = \frac{0.9 \times 0.1542}{\beta \times \cos \theta}$$

where  $D$  is the crystallite size;  $\theta$ , the diffraction angle; and  $\beta = \beta_{\text{exp}} - \beta_{\text{app}}$ . Here,  $\beta_{\text{exp}}$  and  $\beta_{\text{app}}$  are the FWHM of the diffraction peak and the instrumental broadening width, respectively. The specific surface area was calculated using

the BET single-point method from nitrogen uptake measured at  $77\text{ K}$  by using a Micromeritics FlowSorb II 2300 sorption-meter. The samples were pretreated in a  $\text{N}_2$  flow at  $300\text{ }^\circ\text{C}$  for 30 min prior to the measurements. The apparent shape and size of the catalyst particles were observed using a Hitachi S-2500 CX scanning electron microscope (SEM). The catalysts were also characterized by temperature-programmed reduction with  $\text{H}_2$  ( $\text{H}_2$ -TPR). A portion ( $0.010\text{ g}$ ) of a sample was set in a reactor, activated at  $500\text{ }^\circ\text{C}$  for 1 h in an Ar flow and cooled to room temperature. Hydrogen (2 vol%  $\text{H}_2$ -Ar;  $20\text{ cm}^3\text{ min}^{-1}$ ) was introduced to the reactor and the sample was heated at a rate of  $5\text{ }^\circ\text{C min}^{-1}$  up to  $600\text{ }^\circ\text{C}$ . The hydrogen content in the effluent gas from the reactor was measured by a TCD detector of a Shimadzu GC-8A gas chromatograph. Temperature-programmed desorption (TPD) of  $\text{O}_2$  was also carried out in the fixed-bed flow reactor. The pretreatment conditions were the same as in the case of the catalyst tests ( $500\text{ }^\circ\text{C}$ , 30 min in He). After the heat treatment in the helium flow, the temperature of the catalyst bed was decreased to  $50\text{ }^\circ\text{C}$ . The sample was kept at  $50\text{ }^\circ\text{C}$  in a flow of gas composed of 2%  $\text{O}_2$  with helium balance ( $W/F = 0.3\text{ g s cm}^{-3}$ ) for 1 h, and then purged with He ( $100\text{ cm}^3\text{ min}^{-1}$ ) for 1 h. After the treatment, the temperature was raised to  $500\text{ }^\circ\text{C}$  at a rate of  $5\text{ }^\circ\text{C min}^{-1}$  in the helium flow, and the effluent gas from the reactor was continuously analyzed with a Pfeiffer Vacuum Omnistar GSD 301 O 1 quadrupole mass spectrometer. The XPS measurements were carried out with an ULVAC-PHI model 5500 spectrometer with Mg  $\text{K}\alpha$  emission (15 kV, 400 W) as the X-ray source. The binding energy was corrected by the contaminated carbon ( $284.6\text{ eV}$ ) [48].

## Results and discussion

### Effects of the preparation methods on the properties of the catalysts

In order to examine effect of the preparation method on the activity for  $\text{N}_2\text{O}$  decomposition, six K-doped  $\text{Co}_3\text{O}_4$  catalysts were prepared by various methods described in “[Experimental section](#)”. The homogeneous precipitation method via urea hydrolysis has been applied for the preparation of various materials. It was reported that the BET surface areas of  $\text{CeO}_2$ - $\text{ZrO}_2$  catalysts prepared by this method are reasonably large [44].  $\text{Lu}_{1.98}\text{Ln}_{0.02}\text{O}_3$  ( $\text{Ln} = \text{Nd, Eu, and Er}$ ) powders obtained by propellant synthesis via combustion with glycine were reported to have a very porous, open morphology [45]. Free-standing  $\text{Co}_3\text{O}_4$  nanocubes with a uniform size of ca. 47 nm have been prepared by the gradual oxidation method [46]. The  $\text{Co}_3\text{O}_4$  nanorods with a porous structure were obtained

through the thermal treatment of  $\text{Co}(\text{CO}_3)_{0.35}\text{Cl}_{0.20}(\text{OH})_{1.10}$  prepared by hydrothermal reaction of  $\text{CoCl}_2$  with urea [47].

The catalysts were characterized by XRD, SEM,  $\text{H}_2$ -TPR,  $\text{O}_2$ -TPD, nitrogen adsorption/desorption, and XPS to investigate the effects of the preparation methods on the properties of the catalysts. Figure 1 shows the XRD patterns of the precursors of the K/ $\text{Co}_3\text{O}_4$  catalysts, and the phases detected by XRD are summarized in Table 1. The XRD pattern of the precursor obtained by the homogeneous precipitation method (catalyst B) was assigned to a hydroxalcite-like phase [49]. The XRD study also revealed that a mixture of the crystalline  $\text{Co}_3\text{O}_4$  and  $\text{CoO}$  was obtained by the combustion method (JCPDS Cards No. 9-418 and 9-402, respectively) (catalyst C), while hydrothermal reaction of  $\text{CoCl}_2$  with urea yielded  $\text{Co}(\text{CO}_3)_{0.35}\text{Cl}_{0.20}(\text{OH})_{1.10}$  (JCPDS Card No. 38-547) (catalyst E). The XRD pattern of the precursor obtained by gradual oxidation method (catalyst D) is attributed to crystalline  $\text{Co}_3\text{O}_4$ ,  $\text{Co}(\text{OH})_2(\text{NO}_3)_x \cdot n\text{H}_2\text{O}$  and  $\text{Co}(\text{OH})_{2-x}(\text{NO}_3)_x \cdot n\text{H}_2\text{O}$  phases [46].

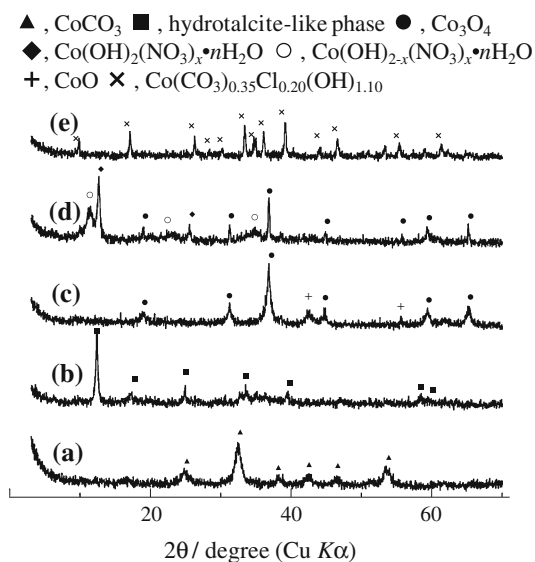


**Fig. 1** XRD patterns of the precursors: (a) catalyst A, (b) catalyst B, (c) catalyst C, (d) catalyst D, (e) catalyst E

**Table 1** Precursor phase for XRD patterns

Catalyst	Co salt source	Synthesis method	Precursor phase
A	Cobalt(II) carbonate	Impregnation	$\text{CoCO}_3$
A'	Cobalt(II,III) oxide	Impregnation	$\text{Co}_3\text{O}_4$
B	Cobalt nitrate hexahydrate	Homogeneous precipitation	Hydroxalcite-like
C	Cobalt nitrate hexahydrate	Combustion with glycine	$\text{Co}_3\text{O}_4$ , $\text{CoO}$
D	Cobalt nitrate hexahydrate	Gradual oxidation	$\text{Co}_3\text{O}_4$ , $\text{Co}(\text{OH})_2(\text{NO}_3)_x \cdot n\text{H}_2\text{O}$ , $\text{Co}(\text{OH})_{2-x}(\text{NO}_3)_x \cdot n\text{H}_2\text{O}$
E	Cobalt chloride hexahydrate	Hydrothermal	$\text{Co}(\text{CO}_3)_{0.35}\text{Cl}_{0.20}(\text{OH})_{1.10}$

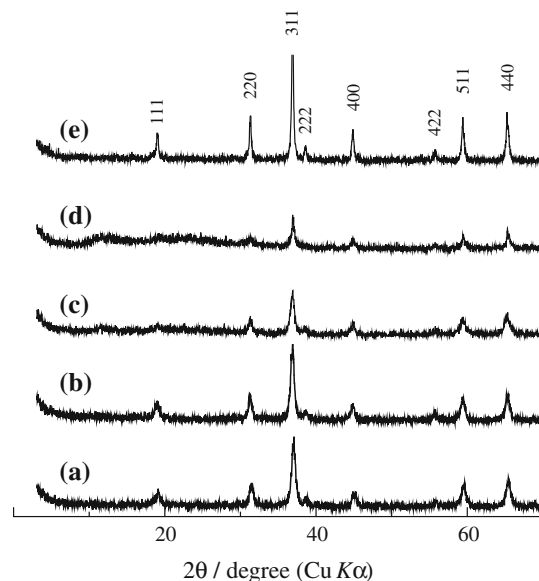


**Fig. 2** XRD patterns of K-doped  $\text{Co}_3\text{O}_4$  catalysts: (a) catalyst A, (b) catalyst B, (c) catalyst C, (d) catalyst D, (e) catalyst E

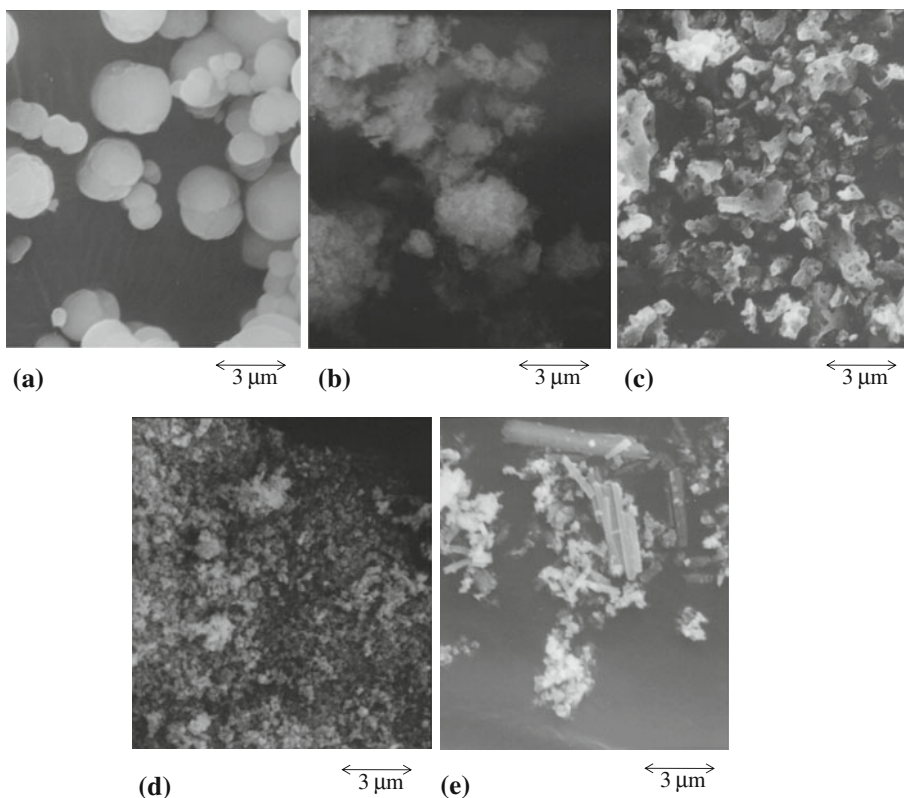
Figure 2 shows the XRD patterns of K-doped  $\text{Co}_3\text{O}_4$  catalysts after the calcination. All the XRD peaks are due to crystalline  $\text{Co}_3\text{O}_4$ . As shown in Table 2, crystallite size of the  $\text{Co}_3\text{O}_4$  phase of catalysts A, B, and C were relatively small, whereas those of catalysts D and E were significantly large. Because the temperature at which the catalysts were pretreated prior to the catalytic runs is higher than the calcination temperature of the samples characterized, data for both the fresh and spent catalysts are given in Table 2. Although the BET surface area of each catalyst decreased by the pretreatment (Table 2), it was significantly affected by the preparation method, and decreased in the following order; catalyst A > B > D > E > C. Catalyst C had a surface area much smaller than that expected from the crystallite size, indicating that the primary particles were severely aggregated.

The extent of the aggregation of primary particles is obvious through the SEM observation as well (Fig. 3). Whereas catalyst C had large pores, the surface of the particles was very smooth, indicating severe aggregation of

**Table 2** Crystallite sizes and BET surface areas of K-doped Co<sub>3</sub>O<sub>4</sub> catalysts

Catalyst	Fresh catalyst		Spent catalyst	
	Crystallite size (nm)	BET surface area (m <sup>2</sup> /g)	Crystallite size (nm)	BET surface area (m <sup>2</sup> /g)
<b>A</b>	22	56	25	36
<b>B</b>	25	39	20	29
<b>C</b>	21	14	31	14
<b>D</b>	56	27	63	24
<b>E</b>	55	18	63	15

**Fig. 3** SEM photographs of K-doped Co<sub>3</sub>O<sub>4</sub> catalysts: **a** catalyst **A**, **b** catalyst **B**, **c** catalyst **C**, **d** catalyst **D**, **e** catalyst **E**



primary particles, in consistent with the discussion mentioned above. Catalyst **E** was composed of nanorods with smooth surface. Catalysts **B** and **D** were comprised of small particles. On the other hand, the catalyst **A** was composed of large spherical aggregates of fine particles.

The results for XPS data are summarized in Table 3. All the catalysts exhibited the peak due to Co 2p<sub>3/2</sub> at binding energy of 779.6–780.1 eV, which was in reasonable agreement with the reported data (779.8 eV) for Co<sub>3</sub>O<sub>4</sub> [50, 51]. It is rather surprising to know that the K/Co ratios in the surface region of catalysts **A** and **C** were rather high in spite of the fact that the former catalyst had a relatively large surface area. This result seems to connect with the morphology of the precursor particles which were essentially identical with the morphology of the catalysts (Fig. 3). Since we impregnated the precursors with a KNO<sub>3</sub>

**Table 3** XPS results for the catalysts

Catalyst	Co 2p <sub>3/2</sub> Binding energy (eV)	Surface composition		
		K/Co	Other element (X) detected	X/Co
<b>A</b>	779.7	0.116	–	–
<b>B</b>	780.0	0.077	–	–
<b>C</b>	779.6	0.108	–	–
<b>D</b>	779.8	0.059	Na	0.493
<b>E</b>	780.1	0.039	Cl	0.071

solution, the promoter is enriched on the outer surface of the particles, and large precursor particles such as CoCO<sub>3</sub> gave high K/Co ratios because the XPS analysis also gives



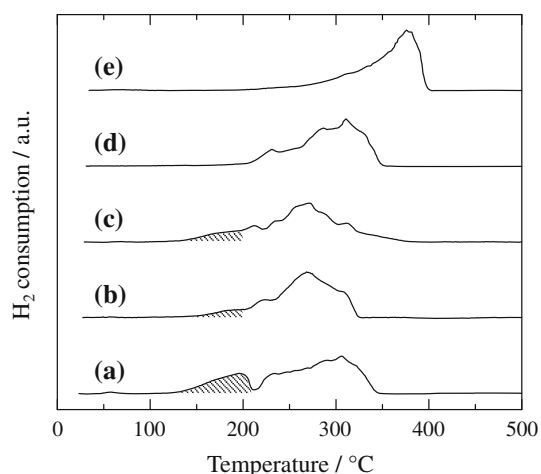


**Fig. 4** H<sub>2</sub>-TPR profiles of K-doped Co<sub>3</sub>O<sub>4</sub> catalysts: (a) catalyst A, (b) catalyst B, (c) catalyst C, (d) catalyst D, (e) catalyst E

the data for the composition at the surface region of the aggregated particles.

The effects of preparation methods on the reduction behavior of the K-doped Co<sub>3</sub>O<sub>4</sub> catalysts were investigated by the H<sub>2</sub>-TPR technique (Fig. 4). For catalyst A, two reduction peaks were observed at around 200 and 250–400 °C. The former peak is attributed to the reduction of Co<sup>3+</sup> to Co<sup>2+</sup>, while the latter is due to the reduction of Co<sup>2+</sup> to Co metal [33, 35, 52, 53]. The hydrogen consumption at <200 °C, as indicated by shadow in Fig. 4, was much significant for catalyst A, less pronounced for catalysts B and C. On the other hand, catalysts D and E did not show distinct hydrogen consumption in this temperature range, suggesting that the reduction of Co<sup>3+</sup> to Co<sup>2+</sup> might occur at higher temperatures. In previous studies [33, 35], a good correlation was found between the N<sub>2</sub>O decomposition activity of the catalysts and the intensity of the peak at around 200 °C in the TPR profiles, and the promotion of the regeneration of the Co<sup>2+</sup> species in the catalytic cycle at lower temperatures was proposed to be responsible for the enhanced catalyst activity. The present results clearly indicate that preparation methods of the catalysts significantly affect the extent of the reduction of Co<sup>3+</sup> to Co<sup>2+</sup> at lower temperatures.

Figure 5 shows the O<sub>2</sub>-TPD profiles of the K/Co<sub>3</sub>O<sub>4</sub> catalysts prepared by various methods. The desorption peaks were observed at 50–180 °C and above 400 °C. The former and latter peaks are assigned to the desorption of adsorbed oxygen and elimination of lattice oxygen, respectively [33]. Catalysts A, B, C, and D showed an oxygen desorption peak at <180 °C. Meanwhile, the intensity of this peak decreased in the order A > B > C > D. On the other hand, catalyst E did not show any peak at such temperature range. Previous study [33] suggested that the number of oxygen adsorption sites

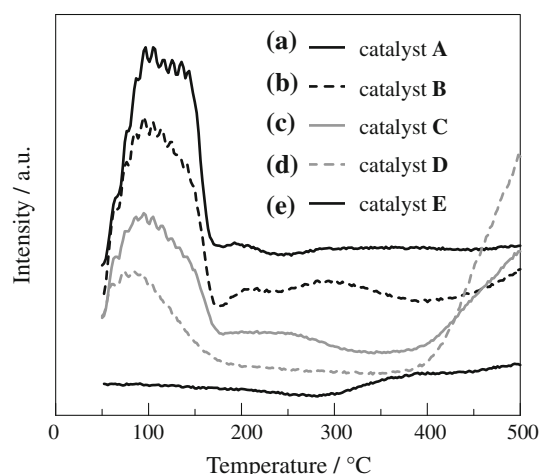


**Fig. 5** O<sub>2</sub>-TPD profiles of K-doped Co<sub>3</sub>O<sub>4</sub> catalysts prepared by various methods

correlates with the activity of the catalyst: The catalyst with higher activity for N<sub>2</sub>O decomposition adsorbs a larger amount of oxygen exhibiting a large desorption peak at <180 °C. For the active catalysts, the deactivation caused by irreversible adsorption of oxygen on the catalyst surface [3, 5, 33] would be suppressed even in the presence of molecular oxygen.

Based on these results, the catalysts prepared in the present study can be classified into two categories: Catalysts A, B, and C belong to the first category. These catalysts exhibited significant hydrogen consumption at <200 °C in H<sub>2</sub>-TPR profiles and adsorbed large amounts of molecular oxygen. Catalysts D and E belong to the second category. These catalysts did not exhibit hydrogen consumption at <200 °C and adsorbed small or negligible amounts of molecular oxygen. The crystallite sizes of the catalysts in the first category were relatively small, while

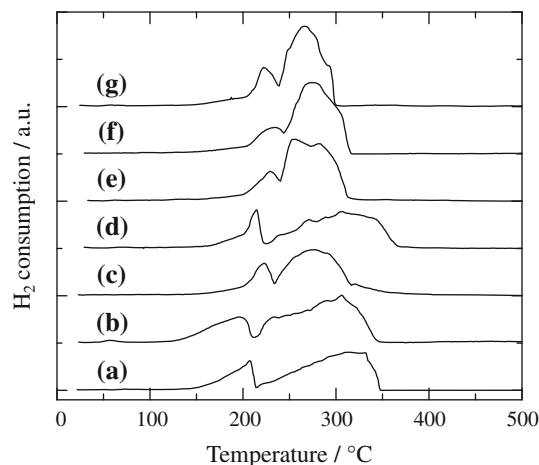


**Fig. 6** H<sub>2</sub>-TPR profiles of Co<sub>3</sub>O<sub>4</sub> catalysts modified by: (a) KOH, (b) KNO<sub>3</sub>, (c) KHCO<sub>3</sub>, (d) CH<sub>3</sub>COOK, (e) K<sub>2</sub>SO<sub>4</sub>, (f) KCl, (g) unpromoted Co<sub>3</sub>O<sub>4</sub>

those of the catalysts in the second category were much larger.

Effects of potassium sources on the reduction behavior of the K-doped  $\text{Co}_3\text{O}_4$  catalyst were examined. Figure 6 shows the  $\text{H}_2$ -TPR profiles of the catalysts prepared by impregnation of commercial cobalt(II) carbonate with various K salts followed by the calcination at 400 °C for 4 h. Again, there were two reduction peaks at around 200 and 250–400 °C, and the former peak was significant for the catalysts prepared using (a) KOH, (b)  $\text{KNO}_3$ , (c)  $\text{KHCO}_3$ , and (d)  $\text{CH}_3\text{COOK}$ , while the catalysts prepared using (e)  $\text{K}_2\text{SO}_4$  and (f) KCl exhibited the peak at  $\sim 230$  °C. Since unpromoted  $\text{Co}_3\text{O}_4$  showed the peak at  $\sim 220$  °C, thermally stable K precursors may have negative effect on reduction of the  $\text{Co}_3\text{O}_4$  catalyst.

Effects of the preparation methods on the catalytic activity of  $\text{K}/\text{Co}_3\text{O}_4$  for  $\text{N}_2\text{O}$  decomposition

The  $\text{N}_2\text{O}$  decomposition activities of the K-doped  $\text{Co}_3\text{O}_4$  catalysts were compared under the dry conditions and the results are shown in Fig. 7. The catalytic activity decreased according to the following order: catalyst  $\mathbf{A} \approx \mathbf{A}' > \mathbf{B} > \mathbf{C} > \mathbf{D} \gg \mathbf{E}$ . Such activity order matches well with the information abstracted from Fig. 5. For catalysts  $\mathbf{A}$  and  $\mathbf{A}'$ ,  $\text{N}_2\text{O}$  conversion to  $\text{N}_2$  at 200 °C was  $>80\%$ . These results indicate that the order of the impregnation of  $\text{KNO}_3$  and the decomposition of cobalt(II) carbonate does not affect the catalytic activity. On the other hand, catalyst  $\mathbf{E}$  had an extremely low activity, and  $\text{N}_2\text{O}$  conversion was  $<10\%$  even at 500 °C. In this respect, XPS study revealed that a significant amount of  $\text{Cl}^-$  ( $\text{Cl}/\text{Co} = 0.071$ ) was remaining on the surface of catalyst  $\mathbf{E}$  (Table 3).

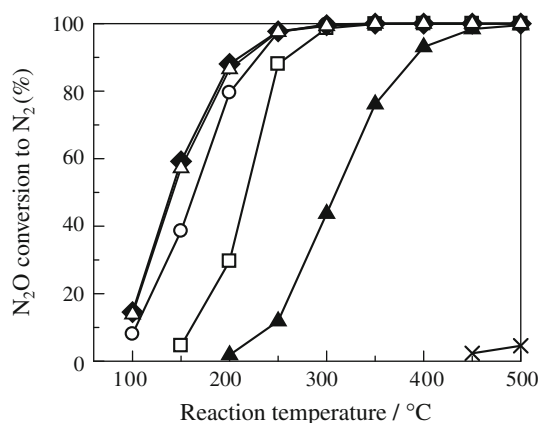


**Fig. 7**  $\text{N}_2\text{O}$  decomposition activities of  $\text{K}/\text{Co}_3\text{O}_4$  catalysts: filled diamond catalyst  $\mathbf{A}$ , open triangle catalyst  $\mathbf{A}'$ , open circle catalyst  $\mathbf{B}$ , open square catalyst  $\mathbf{C}$ , filled triangle catalyst  $\mathbf{D}$ , cross catalyst  $\mathbf{E}$ , under dry conditions. Reaction conditions:  $\text{N}_2\text{O}$ , 5,000 ppm;  $\text{O}_2$ , 2%; He balance;  $W/F = 0.30 \text{ g s cm}^{-3}$

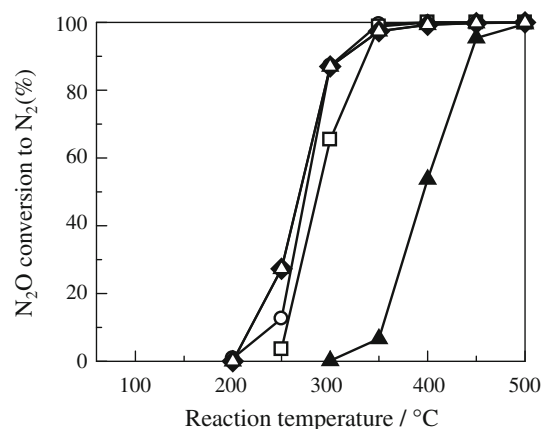


**Fig. 8**  $\text{N}_2\text{O}$  decomposition activities of  $\text{K}/\text{Co}_3\text{O}_4$  catalysts: filled diamond catalyst  $\mathbf{A}$ , open triangle catalyst  $\mathbf{A}'$ , open circle catalyst  $\mathbf{B}$ , open square catalyst  $\mathbf{C}$ , filled triangle catalyst  $\mathbf{D}$ , under wet conditions. Reaction conditions:  $\text{N}_2\text{O}$ , 5,000 ppm;  $\text{O}_2$ , 2%;  $\text{H}_2\text{O}$ , 2.5%; He balance;  $W/F = 0.30 \text{ g s cm}^{-3}$

The catalytic activities for  $\text{N}_2\text{O}$  decomposition were markedly influenced by water present in the feed as shown in Fig. 8. This result suggests that water molecules adsorbed on the active sites hamper the  $\text{N}_2\text{O}$  decomposition. However, the order of activity of the catalysts under the wet conditions was the same as that found under the dry conditions. In Fig. 8, the data for catalyst  $\mathbf{E}$  is not given because it did not exhibit a measurable  $\text{N}_2\text{O}$  decomposition activity even at 500 °C. Catalyst  $\mathbf{A}$  showed the highest activity among the catalysts examined in this study and the activity of this catalyst was maintained at least for 12 h even in the presence of oxygen and water in the feed.

The effect of the K sources on the activities of the catalysts prepared by the impregnation of cobalt(II)

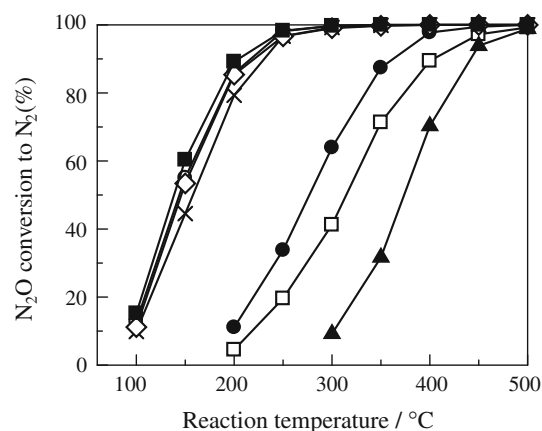


**Fig. 9**  $\text{N}_2\text{O}$  decomposition activities of  $\text{Co}_3\text{O}_4$  catalysts modified by: filled square KOH, open diamond  $\text{KNO}_3$ , open circle  $\text{KHCO}_3$ , cross  $\text{CH}_3\text{COOK}$ , filled circle  $\text{K}_2\text{SO}_4$ , open square KCl, filled triangle without K modification, under dry conditions. Reaction conditions:  $\text{N}_2\text{O}$ , 5,000 ppm;  $\text{O}_2$ , 2%; He balance;  $W/F = 0.30 \text{ g s cm}^{-3}$

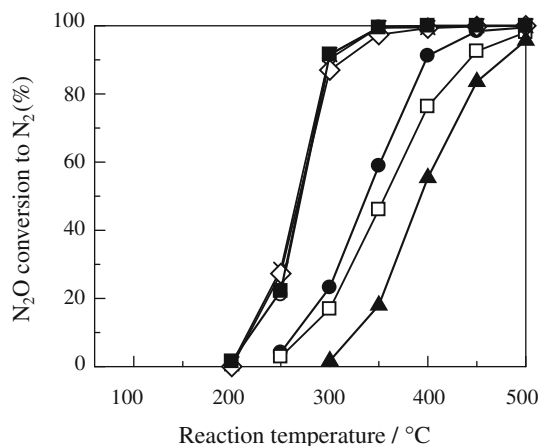


**Fig. 10** N<sub>2</sub>O decomposition activities of Co<sub>3</sub>O<sub>4</sub> catalysts modified by: filled square KOH, open diamond KNO<sub>3</sub>, open circle KHCO<sub>3</sub>, cross CH<sub>3</sub>COOK, filled circle K<sub>2</sub>SO<sub>4</sub>, open square KCl, filled triangle without K modification, under wet conditions. Reaction conditions: N<sub>2</sub>O, 5,000 ppm; O<sub>2</sub>, 2%; H<sub>2</sub>O, 2.5%; He balance; W/F = 0.30 g s cm<sup>-3</sup>

carbonate followed by calcination was examined. Figure 9 shows that the results of the reactions under the dry conditions. The catalytic activity decreased according to the following order: KOH > KNO<sub>3</sub> ≈ KHCO<sub>3</sub> > CH<sub>3</sub>COOK ≫ K<sub>2</sub>SO<sub>4</sub> > KCl. Under the wet conditions, their activities again markedly decreased as shown in Fig. 10. However, the order of the activity was basically unchanged, and the differences in the activities between the catalysts modified with KOH, KNO<sub>3</sub>, KHCO<sub>3</sub>, and CH<sub>3</sub>COOK were negligible. On the other hand, the catalysts prepared by using K<sub>2</sub>SO<sub>4</sub> and KCl showed low activities. The presence of sulfates (0.6 at.%) and Cl<sup>-</sup> ions (2 at.%) in the surface region of the catalyst particles was confirmed by XPS analysis. It is interesting to note that the activities of K<sub>2</sub>SO<sub>4</sub>- and KCl-modified catalysts were higher than that of the unpromoted Co<sub>3</sub>O<sub>4</sub> catalyst. This result indicates that K<sup>+</sup> ions derived from the hardly decomposable salts also have the promoting effect on the Co<sub>3</sub>O<sub>4</sub> catalyst to some extent.

The combined results of the characterization and catalytic runs clearly show the close correlation between the redox behavior and the activity of the catalysts. The catalyst having easily reducible Co<sup>3+</sup> species which adsorbed a large amount of molecular oxygen (exhibited an intense desorption peak at <180 °C in the O<sub>2</sub>-TPD profile) showed an excellent activity for N<sub>2</sub>O decomposition. On the contrary, the catalyst having only hardly reducible Co<sup>3+</sup> species showed a low activity. Possible reason for extremely poor activity of catalyst E would be Cl<sup>-</sup> ion remaining on the surface of the catalyst. Note that the crystallite sizes of the active catalysts were relatively small (see above). A large number of surface defects such as steps and kinks were exposed on the surface of the crystallites with smaller

sizes. Recently, Xu et al. [54] studied the reaction mechanisms for catalytic oxidation of CO by N<sub>2</sub>O on Co<sub>3</sub>O<sub>4</sub>(110) surfaces by DFT slab calculations, and found that N<sub>2</sub>O reacts with the oxygen vacancy on the defect Co<sub>3</sub>O<sub>4</sub>(110) surface yielding N<sub>2</sub> and perfect Co<sub>3</sub>O<sub>4</sub>(110) surface. The reactions of N<sub>2</sub>O with the surface oxygen vacancies are well known [55–59]. For example, Henderson et al. [57] found that oxygen vacancies on TiO<sub>2</sub>(110), formed by annealing TiO<sub>2</sub>(110) surface in vacuum at >800 K, react with N<sub>2</sub>O even at 90 K resulting in ejection of N<sub>2</sub> and vacancy oxidation. However, such a process is not always catalytic, and Xu et al. [54] found that interaction between N<sub>2</sub>O and perfect Co<sub>3</sub>O<sub>4</sub>(110) surface is quite weak, whereas oxygen vacancy is regenerated by the reaction of perfect Co<sub>3</sub>O<sub>4</sub>(110) surface with CO, a strong reducing agent. In the present study, such a reducing agent is absent, and therefore, the reaction of N<sub>2</sub>O with oxygen vacancies is not involved in the catalytic cycle of the present catalyst system. Instead, we believe that surface defects such as steps and kinks act as the N<sub>2</sub>O adsorption sites, where heat of adsorption of N<sub>2</sub>O would be much smaller than that evolved when N<sub>2</sub>O is adsorbed on oxygen vacancies. However, surface defects would be easily regenerated by desorption of O<sub>2</sub>, which permit the catalytic cycle for N<sub>2</sub>O decomposition. Since the adsorption of atomic oxygen on the defect site is accompanied with the oxidation of Co<sup>2+</sup> located in the defect, such Co<sup>2+</sup> ions can be considered as the active sites for the N<sub>2</sub>O decomposition through the redox mechanism [33, 36, 38, 40, 60–64].

The K<sup>+</sup> species on the catalysts were proposed to destabilize the oxygen atoms formed by the cleavage of N–O bond of N<sub>2</sub>O, and thus promote desorption of oxygen molecules from the catalysts to regenerate the catalytically active species [33]. The results in the present study support this idea, but the effect of K-doping was found to be significantly influence by the counter anions. The use of K<sub>2</sub>SO<sub>4</sub> and KCl was less effective. These results may be caused by sulfate and Cl<sup>-</sup> ions remaining on the catalyst surface, because these anions are strongly adsorbed on the surface defects, thus hampering the N<sub>2</sub>O decomposition reaction.

## Conclusions

The activity of K/Co<sub>3</sub>O<sub>4</sub> catalysts for the direct decomposition of nitrous oxide was greatly affected by both the preparation methods and potassium sources. Among the catalysts examined, the catalyst prepared by impregnation of CoCO<sub>3</sub> with an aqueous solution of KOH showed the highest activity. The catalysts with smaller crystallite sizes generally showed higher activities. Chloride and sulfate ions remaining on the surface of the catalysts greatly



inhibited their activities. The intensity of the O<sub>2</sub>-desorption peak at <180 °C in O<sub>2</sub>-TPD experiment was found to be a good diagnosis of the activity of the catalyst. The TPR measurements revealed that preparation methods of the catalysts as well as potassium sources significantly influenced the extent of the reduction of Co<sup>3+</sup> to Co<sup>2+</sup> at low temperature (~200 °C), which crucially affect the activity for N<sub>2</sub>O decomposition.

## References

- IPCC Third Assessment Report – Climate Change 2001: The Scientific Basis, The Intergovernmental Panel on Climate Change, Working Group I. Original report is available at: [http://www.grida.no/publications/other/ipcc%5Ftar/?src=/climate/ipcc\\_tar/wg1/index.htm](http://www.grida.no/publications/other/ipcc%5Ftar/?src=/climate/ipcc_tar/wg1/index.htm)
- Kapteijn F, Rodriguez-Mirasol J, Moulijn JA (1996) Appl Catal B: Environ 9:25
- Centi G, Galli A, Montanari B, Perathoner S, Vaccari A (1997) Catal Today 35:113
- Haber J, Machej T, Janas J, Nattich M (2004) Catal Today 90:15
- Tzitzios VK, Georgakilas V (2005) Chemosphere 59:887
- Haber J, Nattich M, Machej T (2008) Appl Catal B: Environ 77:278
- Drago RS, Jurczyk K, Kob N (1997) Appl Catal B: Environ 13:69
- Satsuma A, Maeshima H, Watanabe K, Suzuki K, Hattori T (2000) Catal Today 63:347
- Scagnelli A, di Valentin C, Pacchioni G (2006) Surf Sci 600:386
- Russo N, Mescia D, Fino D, Saracco G, Specchia V (2007) Ind Eng Chem Res 46:4226
- Pasha N, Lingaiah N, Reddy PSS, Prasad PSS (2009) Catal Lett 127:101
- da Cruz RS, Mascarenhas AJS, Andrade HMC (1998) Appl Catal B: Environ 18:223
- Pérez-Ramírez J, Kapteijn F, Mul G, Moulijn JA (2001) Chem Commun 693
- Guesmi H, Berthomieu D, Kiwi-Minsker L (2008) J Phys Chem C 112:20319
- Zakirov V, Sweeting M, Lawtence T, Sellers J (2001) Acta Astronaut 48:353
- Zakirov V, Zhang H-Y (2008) Aerospace Sci Technol 12:318
- Shimizu A, Tanaka K, Fujimori M (2000) Chemosphere Global Change Sci 2:425
- Shimizu A, Miura K, Tagawa K, Kan H (2004) J Chem Eng Jpn 37:808
- Stelmachowski P, Zasada F, Maniak G, Granger P, Inger M, Wilk M, Kotarba A, Sojka Z (2009) Catal Lett 130:637
- Schmid G, Keller N (1950) Naturwiss 37:42
- Amphlett CB (1954) Trans Faraday Soc 50:273
- Volpe ML, Reddy JF (1967) J Catal 7:76
- Armor JN, Braymer TA, Farris TS, Li Y, Petrocelli FP, Weist EL, Kannan S, Swamy CS (1996) Appl Catal B: Environ 7:397
- Kannan S, Swamy CS (1999) Catal Today 53:725
- Chellam U, Xu ZP, Zeng HC (2000) Chem Mater 12:650
- Yan L, Ren T, Wang X, Ji D, Suo J (2003) Appl Catal B: Environ 45:85
- Yan L, Ren T, Wang X, Gao Q, Ji D, Suo J (2003) Catal Commun 4:505
- Obalová L, Fila (2007) Appl Catal B: Environ 70:353
- Armor JN, Braymer TA, Li Y, Farris TS (1995) USP 005472677 (Engelhard Co)
- Pérez-Ramírez J, Garecía-Cortés JM, Kapteijn F, Illán-Gómez MJ, Ribera A, de Lecea CS-M, Moulijn JA (2000) Appl Catal B: Environ 25:191
- Ohnishi C, Asano K, Iwamoto S, Inoue M (2006) Stud Surf Sci Catal 162:737
- Ohnishi C, Asano K, Iwamoto S, Chikama K, Inoue M (2007) Catal Today 120:145
- Asano K, Ohnishi C, Iwamoto S, Shioya Y, Inoue M (2008) Appl Catal B: Environ 78:242
- Xue L, Zhang C, He H, Teraoka Y (2007) Catal Today 126:449
- Pasha N, Lingaiah N, Babu NS, Reddy PSS, Prasad PSS (2008) Catal Commun 10:132
- Stelmachowski P, Maniak G, Kotarba A, Sojka Z (2009) Catal Commun 10:1062
- Zasada F, Stelmachowski P, Maniak G, Paul J-F, Kotarba A, Sojka Z (2009) Catal Lett 127:131
- Abu-Zied BM, Soliman SA (2009) Catal Lett 132:299
- Cheng H, Huang Y, Wang A, Li L, Wang X, Zhang T (2009) Appl Catal B: Environ 89:391
- Xue L, He H, Liu C, Zhang C, Zhang B (2009) Environ Sci Technol 43:890
- Obalová L, Karásková K, Jiráťová K, Kovanda F (2009) Appl Catal B: Environ 90:132
- Park PW, Kil JK, Kung HH, Kung MC (1998) Catal Today 42:51
- Haneda M, Kintaichi Y, Bion N, Hamada H (2003) Appl Catal B: Environ 46:473
- Pengpanich S, Meeyoo V, Rirksomboon T, Bunyakiat K (2002) Appl Catal A: Gen 234:221
- Polizzi S, Bucella S, Speghini A, Vetrone F, Naccache R, Boyer JC, Capobianco JA (2004) Chem Mater 16:1330
- Xu R, Zeng HC (2003) J Phys Chem B 107:926
- Wang Z, Chen X, Zhang M, Qian Y (2005) Solid State Sci 7:13
- Moulder F, Stickle WF, Sobol PE, Bomben KD (1992) Handbook of X-ray photoelectron spectroscopy. Perkin-Elmer Co, Eden Prairie (USA)
- Xu R, Zeng HC (2003) J Phys Chem B 107:12643
- Haneda M, Nakamura I, Fujitani T, Hamada H (2006) Catal Surv Asia 9:207
- Avila AG, Barrera EC, Huerta LA, Muhl A (2004) Solar Energ Mater Solar Cell 82:269
- Sexton BA, Hughes AE, Turney TW (1986) J Catal 97:390
- Voß M, Borgmann D, Wedler G (2002) J Catal 212:10
- Xu X-L, Yang E, Li J-Q, Li Y, Chen W-K (1991) ChemCatChem 1:384
- Winter ERS (1969) J Catal 15:144
- Cunningham J, Penny AL (1974) J Phys Chem 78:870
- Henderson MA, Szanyi J, Peden CHF (2003) Catal Today 85:251
- Zhu J, Albertsma S, van Ommen JG, Lefferts L (2005) J Phys Chem B 109:9550
- Chen W-K, Sun B-Z, Wang X, Lu C-H (2008) J Theo Comput Chem 7:263
- Dandekar A, Vannice MA (1999) Appl Catal B: Environ 22:179
- Zhu Z, Lu GQ, Zhuang Y, Shen D (1999) Energy Fuels 13:763
- Pinna F, Scarpa M, Strukul G, Guglielminotti E, Bocuzzi F, Manzoli M (2000) J Catal 192:158
- Fanning PE, Vannice MA (2002) J Catal 207:166
- Nobukawa T, Yoshida M, Okumura K, Tomishige K, Kunimori K (2005) J Catal 229:374